SAN096-1682C

EVALUATING MECHANICAL PROPERTIES OF THIN LAYERS USING NANOINDENTATION AND FINITE-ELEMENT MODELING: IMPLANTED METALS AND DEPOSITED LAYERS

SAND--96-1682C

J.A. KNAPP *, D.M. FOLLSTAEDT *, J.C. BARBOUR *, S.M. MYERS *, J.W. AGER **, O.R. MONTEIRO**, AND I.G. BROWN**
*Sandia National Laboratories, Albuquerque, NM 87185
**Lawrence Berkeley National Laboratory, Berkeley, CA 94720

CONF-961202--22

ABSTRACT

We present a methodology based on finite-element modeling of nanoindentation data to extract reliable and accurate mechanical properties from thin, hard films and surface-modified layers on softer substrates. The method deduces the yield stress, Young's modulus, and hardness from indentations as deep as 50% of the layer thickness.

INTRODUCTION

Nanoindentation has become a common tool in the study of mechanical properties on relatively small scales or near surfaces. However, these measurements become less accurate when studying thin layers, especially when the indentation depth is a significant fraction of the layer thickness. In such cases finite-element modeling is required because the nanoindentation response can be strongly influenced by the properties of the underlying substrate and evaluation of the layer properties by analytical methods is not feasible. We have developed procedures using the commercial, large-strain, finite-element code ABAQUS [1] to simulate the nanoindentation response, with utilities to generate meshes specific to each sample and to fit the results [2-4]. Flexibility in mesh generation is important because numerical convergence can be sensitive to details of the sample structure and layer properties. The two parameters for the layer which are extracted from the fit of simulation to experiment are the yield stress (defined at a plastic strain of .002), and Young's modulus. Hardness, a commonly used figure of merit, is then deduced by an additional simulation using the yield stress and elasticity of the layer in a hypothetical bulk "sample". These methods have been applied to a wide range of systems: examples are given from an FeTiC alloy formed by pulsed laser deposition, hard "diamond-like" carbon layers formed using vacuum arc deposition, and Er-implanted Al(O) layers initially formed using an electron cyclotron resonance plasma. Our approach increases the applicability of nanoindentation testing to very thin layers, composite layers, and modulated compositions.

NANOINDENTATION AND FINITE-ELEMENT MODELING

For the nanoindentation measurement [5], a three-sided, Berkovich-shaped diamond indenter is pushed into the sample under very fine depth and load control. The force required during both insertion and extraction is recorded as a function of depth. The force required to indent to a given depth is indicative of the hardness of the material, while the recovery of the material during unloading is indicative of its elastic properties. For bulk samples or relatively thick films, analytical examination of the data directly deduces the hardness and Young's modulus of the material [6]. When the sample is a thin layer on a substrate with different properties, analytical methods are inadequate since the force versus depth response is due to a combination of the layer and substrate properties. To deduce the mechanical properties of the layer alone, we use

MASTER

DISTRIBUTION OF THIS DOCUMENT IS UNLIMITED

DISCLAIMER

This report was prepared as an account of work sponsored by an agency of the United States Government. Neither the United States Government nor any agency thereof, nor any of their employees, make any warranty, express or implied, or assumes any legal liability or responsibility for the accuracy, completeness, or usefulness of any information, apparatus, product, or process disclosed, or represents that its use would not infringe privately owned rights. Reference herein to any specific commercial product, process, or service by trade name, trademark, manufacturer, or otherwise does not necessarily constitute or imply its endorsement, recommendation, or favoring by the United States Government or any agency thereof. The views and opinions of authors expressed herein do not necessarily state or reflect those of the United States Government or any agency thereof.

DISCLAIMER

Portions of this document may be illegible in electronic image products. Images are produced from the best available original document.

finite-element modeling. The mesh is constructed to reflect as accurately as possible the composite sample structure, the properties of the substrate and indenter are fixed at known values, and then simulations of the experiment are performed with different sets of layer properties until a match to the experimental force vs. depth response is obtained. To minimize the number of simulations required before a good fit is obtained, the results are parameterized and compared to experiment so that extrapolations can be made to the layer properties which should give a better fit.

We use the large-strain, finite-element code ABAQUS [1] for our simulations. One advantage of using this widely available commercial code is that our methods can be easily transferred to other laboratories. Other advantages specific to nanoindentation include properly modeling the changing contact between indenter and surface (including sliding with friction), and allowing pre-existing stress in the layers to be specified. There are two solvers presently available: ABAQUS/Standard, a direct solver ideal for quasistatic problems, and ABAQUS/Explicit, a solver optimized for dynamic problems with significant kinetic energy and inertial effects. Our earlier work [2-3] with ABAQUS also used a beta-version conjugate gradient solver optimized for larger quasistatic problems, but this solver is no longer available. A set of typical simulations has been run on all three solvers: each solver gave identical results (force vs. depth response curves), but with significant differences in speed and stability [4]. Simulations can be performed with either a 3-dimensional sample mesh or with a 2-dimensional axisymmetric mesh, where the pyramid-shaped indenter is approximated by a cone-shaped indenter with the same cross-sectional area versus depth. In each case we have examined, a 2-dimensional simulation gives results very close to those from a full 3-dimensional simulation, so for computational efficiency we generally limit the analyses to 2 dimensional simulations. We now use ABAQUS/Standard for all these simulations. A typical simulation with 6000 elements runs in 30-40 minutes using Standard on a desktop workstation. It would take about twice as long with the conjugate gradient solver and several hours with the Explicit dynamic solver. (The dynamic solver can be used for these quasistatic simulations by scaling the indent speed up to a point where the solution time is acceptable, but not so high that total kinetic energy is more than a small fraction of the total energy).

Figure 1 shows a flowchart of the overall process. The problem setup is done with two utilities written in Visual Basic™ on a desktop computer. The first utility generates the mesh definition list, using the calibration function determined by an indentation procedure to properly

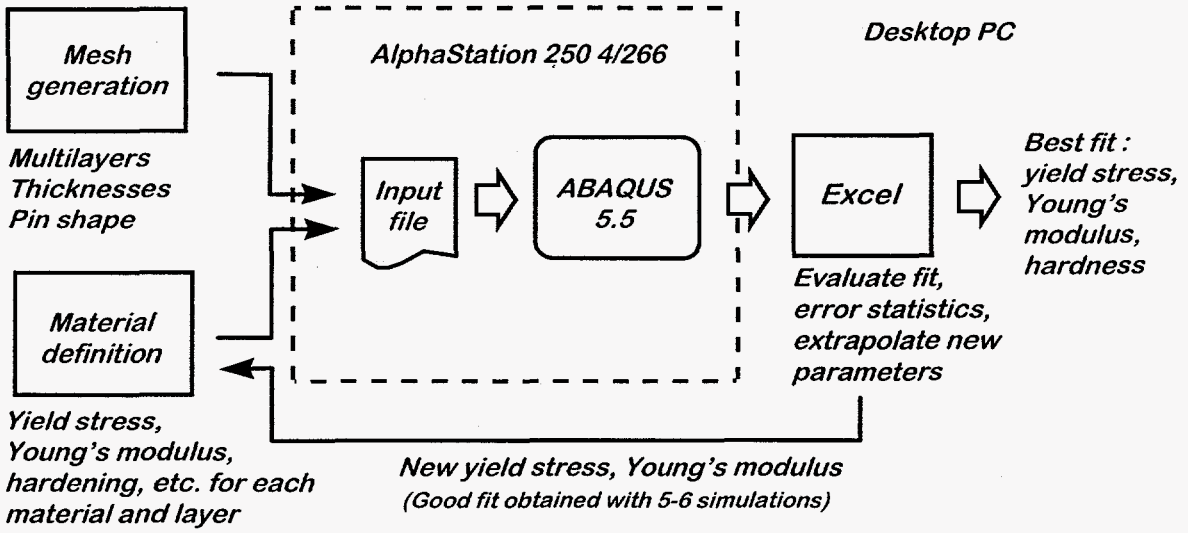

Figure 1. Flowchart of the simulation procedure.

define the indenter shape. Layer thickness is input by the user and the output is a text file suitable for incorporation in the ABAQUS input file. The second utility accepts the desired material properties (yield stress, Young's modulus, etc.) for each part of the model and generates a definition of the stress-strain relationship for each, along with other commands needed to define the materials for ABAQUS. These two text files are transferred to the Unix workstation and combined with other commands (depths, output requests, etc.) to form an ABAQUS input file, which is then used to run the simulation. The different parts of the input file are generated separately and then combined on the workstation since generally only the layer material definitions are varied during a series of simulations for a single sample. Usually only the yield stress and Young's modulus of the layer are changed, with the work hardening rate fixed at a value typical of the material being studied.

After each simulation several Mbytes of output data are archived, while a small subset of data (typically just the force vs. depth history) is extracted and transferred back to the desktop computer. Using an Excel™ spreadsheet, both the experimental and simulated force vs. depth curves are parameterized so that an extrapolation can be made to the next values of layer yield stress and Young's modulus to be tried [3,4]. In the simplest case, two parameters are used, the loading force at some fixed depth and the initial slope of the unloading. Both are dependent on the values of yield stress and Young's modulus, a dependency which we have shown to be approximately linear for small changes. Thus, once 3 or 4 simulations using different values of yield stress and Young's modulus (selected to approximately bracket the expected experimental values) have been obtained, it is straightforward using the average experimental force and slope to extrapolate to a new yield stress and Young's modulus which should give a good fit to the experiment. These new values are fed back into the material definition utility and an input file is generated for a new simulation. Generally, a good fit to the experiment can be obtained within 5 or 6 simulations.

The parameterization of the simulation and experimental curves is also useful in quantifying the total error in the final values of yield stress and Young's modulus. First, the variation in the 8-10 experimental indents is evaluated and the statistics of this data set are used with the extrapolation functions to give errors for the derived yield stress and Young's modulus. The error which results from any non-linearity in this extrapolation is also included. To account for how well the overall curve shape fits the experiment through the entire loading section, the fit and extrapolation of yield stress and Young's modulus is performed at three different fixed depths and the errors averaged.

Figure 2 shows the central portion of a typical 2-dimensional axisymmetric mesh with the indenter at 160 nm depth. The layer thickness for this sample, to be discussed next, is only 290 nm, so the indent depth is more than 50% of the layer thickness. Close examination of the indenter tip will show the slight blunting which is typical for these instruments; the shape of the axisymmetric mesh for the simulated indenter is matched to the

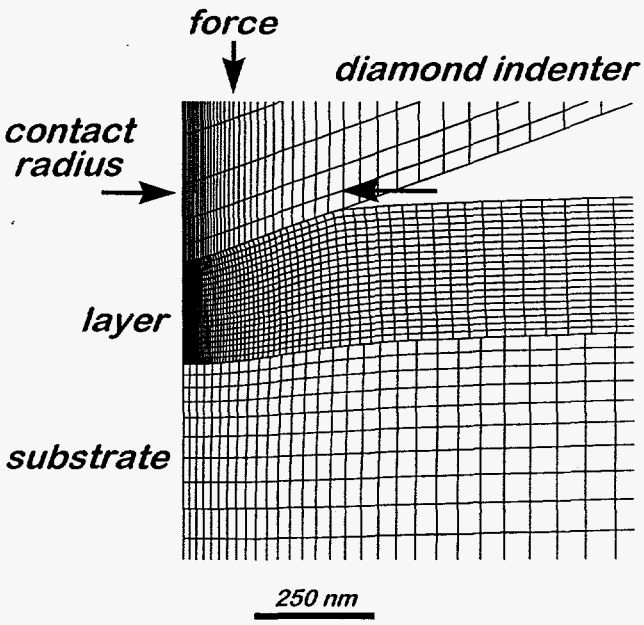

Figure 2. Two-dimensional axisymmetric mesh, used for modeling nanoindentation of $Fe_{64}Ti_{18}C_{18}$ on fused silica.

area vs. depth of the actual indenter using an experimental area calibration, including the small amount of blunting at the tip.

The simulation procedure described above gives a best fit to the experiment and thus derives the yield stress and Young's modulus of the layer material. The apparent hardness of the sample can also be extracted directly from the simulation. Hardness is simply the indent force divided by contact area, so the hardness at each step of the calculation can be derived by outputting the contact radius and force, as noted in Fig. 2. It is important to remember, however, that this is the hardness of the combined layer and substrate, and includes the effects of the substrate. To derive a value of hardness that is intrinsic to the layer material alone requires an additional simulation, where the material properties derived for the layer are used for the entire sample, layer plus substrate.

EXAMPLES

$Fe_{64}Ti_{18}C_{18}$ on fused silica

The first example of the application of these techniques is an amorphous metal layer deposited on fused silica using pulsed laser deposition (PLD) [2]. The alloy is $Fe_{64}Ti_{18}C_{18}$, formed by depositing alternatively from Fe and TiC targets at room temperature, with the ratio of laser shots on the two targets controlling the composition. The amount of material deposited in each sequence was kept to a monolayer or less so that the resulting alloy was uniform in composition. Thickness and composition were measured by Rutherford backscattering spectrometry, while the microstructure was determined by transmission electron microscopy to be amorphous. The alloy is expected to be very similar to those formed when Ti and C are implanted into pure Fe or Fe-based steels [7]. The implantation-formed layers were also amorphous and exhibited very good tribological properties, but the hardness was never accurately determined. The PLD-deposited layer here was 290 nm thick, and a plot of the central portion of the mesh during a simulation has been shown in Fig. 2. The full size of the mesh was

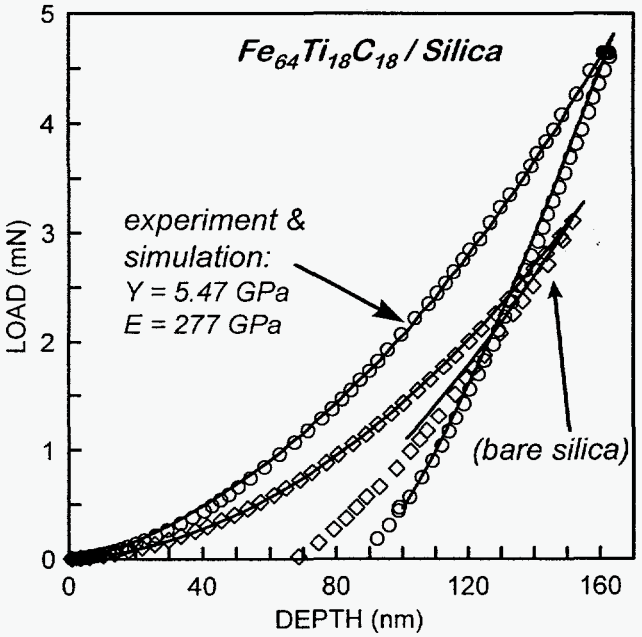

Figure 3. Experimental and calculated nanoindentation curves for bare fused silica and a 290 nm thick, amorphous $Fe_{64}Ti_{18}C_{18}$ alloy deposited by PLD on silica.

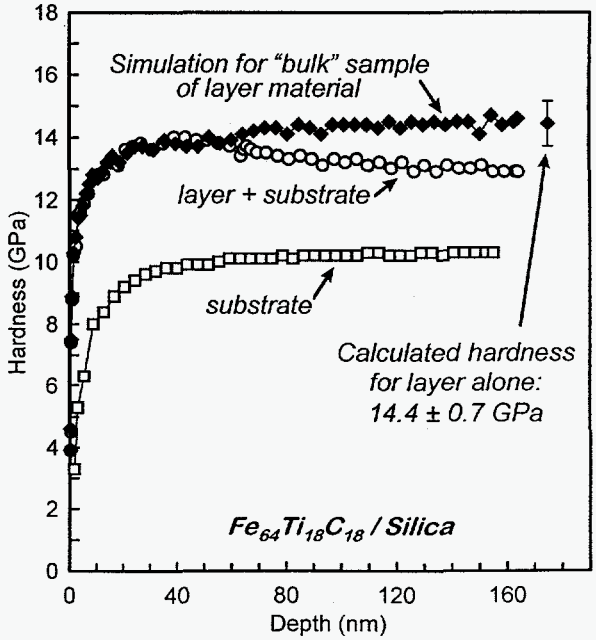

Figure 4. Calculated hardness for bare fused silica, $Fe_{64}Ti_{18}C_{18}$ layer on silica, and a simulated bulk sample of $Fe_{64}Ti_{18}C_{18}$.

15 μm in radius, depth, and indenter thickness. The diamond indenter was modeled as a purely elastic solid (no yielding) with a Young's modulus of 1100 GPa. The fused silica substrate was modeled as an elastic-plastic material with no work hardening using parameters determined by separate nanoindentation and fitting of the base material. Figure 3, which shows the experimental nanoindentation from the $Fe_{64}Ti_{18}C_{18}$ layer, also shows a nanoindentation curve and the best fit simulation for the fused silica substrate alone. The yield stress and Young's modulus determined for the silica substrate were 7.1±0.3 GPa and 73±0.5 GPa, respectively.

The $Fe_{64}Ti_{18}C_{18}$ layer was modeled as an elastic-plastic solid, using the classical metal plasticity model in ABAQUS with a Mises yield surface and associated plastic flow [8]. Poisson's ratio for pure Fe was used, and work hardening was fixed at zero for all simulations, since the amorphous alloy is not expected to show hardening behavior. Initial stress in the layer (tensile or compressive) can also be specified in the simulations, but this had not been measured and was left at zero. Friction between indenter and layer surface was specified at 0.2; simulations have shown that varying the value of friction has essentially no effect on the results. Using all these parameters and those determined for the silica substrate, fitting by the procedure detailed above gave a yield stress for the layer material of 5.47±0.28 GPa and a Young's modulus of 277±14 GPa. The quality of the fit in Fig. 3 for both loading and unloading is very good; note that the unloading part of the simulation does not pass through the experimental points, but has the same slope. The experiments include a short period with the load held constant at the maximum depth; during this time the layer exhibits a small amount of creep, which shifts the experimental unloading curve to deeper depth. Since creep is not modeled by the calculation, the simulated curve is not shifted.

The hardness as a function of depth for the simulations of the silica substrate and the $Fe_{64}Ti_{18}C_{18}$ layer on silica are shown in Fig. 4, along with the hardness calculated for a simulated bulk sample of the layer material alone. The calculated hardness for bulk silica (open squares) converges at depth to a value of 10.23±0.23 GPa, which matches the value of 10.19±0.09 GPa derived directly from the experiment using standard analytical methods [6]. This agreement confirms that the hardness derived from simulation is accurate. The hardness calculated for the layer-plus-substrate combination (open circles) peaks near 40 nm and then falls off at deeper depths, as the effect of the softer substrate increases. As discussed before, to derive an accurate value for the hardness of the layer material alone an additional simulation is performed, using a bulk "sample" with the mechanical properties already derived for the layer material. This calculation for the $Fe_{64}Ti_{18}C_{18}$ alloy is shown by the filled circles in Fig. 4. The hardness converges at depth to a value of 14.4±0.7 GPa. This value is exceptionally high for Fe alloys but is consistent with established trends in rapidly quenched amorphous metals and with evidence of the hardening effect of Ti-C pairing reactions in such materials [9-11].

In the hardness versus depth calculated for the combined layer and substrate, shown as open circles in Fig. 4, the falloff in hardness after 40 nm depth shows again why simulations are needed to properly interpret the data from the nanoindentation of such samples. In this case, evaluating the hardness analytically with an indent depth of only 40 nm would give the correct answer for the layer hardness, since the "bulk" calculated hardness is the same as the combined value at 40 nm. However, for many samples with thinner layers or softer substrates calculations show that the combined hardness does not reach the layer hardness at any depth.

DLC layers on silicon

The next example is a pair of "diamond-like" carbon (DLC) layers formed on silicon using vacuum arc deposition [12-14]. In this technique, C^+ ions were extracted from a vacuum arc plasma, filtered magnetically, and deposited on a substrate which was biased negatively with a 25% duty cycle. The film properties vary with substrate bias: the "hard" film shown here was

deposited with -100 V bias and the "soft" film with -2000 V bias. The "hard" film was 700 nm thick, while the "soft" film was 400 nm thick. These films exhibit high residual compressive stress, which has been measured for the "hard" layer at -10.5 GPa and for the "soft" film at -3.0 GPa. Such pre-existing stress in the layers is known to affect the nanoindentation measurements [15], and another significant value of using ABAQUS for modeling the results is that the initial stress can be specified, if known. We have found that the correction to the derived hardness is generally around 10% of the stress value. Thus 10 GPa compressive stress in a layer makes it appear ~1 GPa harder in a conventional analysis than it would be if unstressed.

Figure 5 shows experimental nanoindentation curves and the best-fit simulations for the two types of DLC films on Si. The DLC films were modeled as elastic-plastic solids, Poisson's ratio for pure diamond was used (0.1), and work hardening was fixed at zero for all simulations. The Si substrate was modeled as an elastic-plastic material with no work hardening using parameters determined again by separate nanoindentation and fitting. The simulations were done with the pre-existing stress in the layers specified, so the derived yield stresses of 49.1±2.9 and 14.1±0.4 GPa are intrinsic to the layers. The derived Young's moduli were 848±10 and 360±10 GPa. The calculated hardnesses vs. depth are shown in Fig. 6: the open symbols are the hardnesses for the best-fit simulations in Fig. 5, i.e. for the layer and substrate combined. Since the "hard" layer is relatively thick, the combined hardness does not fall off significantly with depth, while the combined hardness for the thinner "soft" layer starts to fall off somewhat near 90 nm. The filled symbols in Fig. 6 show the hardnesses calculated for the hypothetical bulk samples of the two layer materials, using the above values for yield stress and Young's modulus, but without any pre-existing stress. The intrinsic hardnesses for the two layer materials are 68.4±2.5 GPa and 27.5±0.7 GPa.

The value of 68.4 GPa for the "hard" film should be compared to an expected hardness for the diamond indenter of ~100 GPa [16]. Indeed, this hardness for the layer is high enough that a concern arises that the diamond indenter may be yielding, which would lead to incorrect results. Normally, the diamond indenter is modeled as a purely elastic solid, i.e. without a yield point. Under those conditions, examination of the calculated stress in the indenter in the simulation of

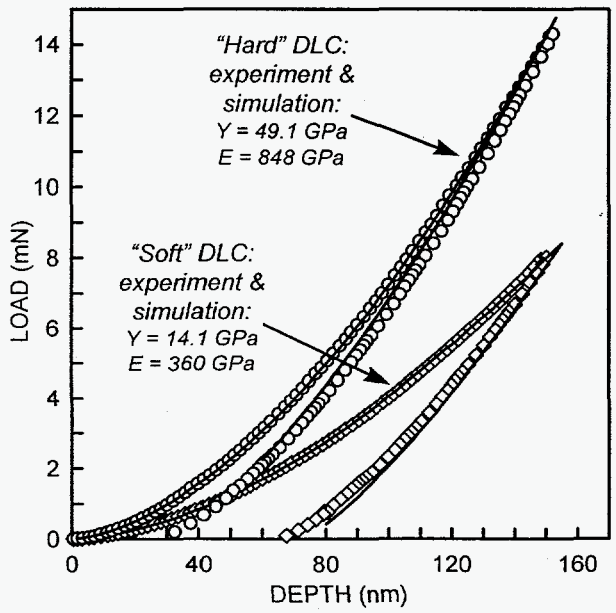

Figure 5. Nanoindentation and simulations for DLC films formed by vacuum arc deposition on a Si substrate.

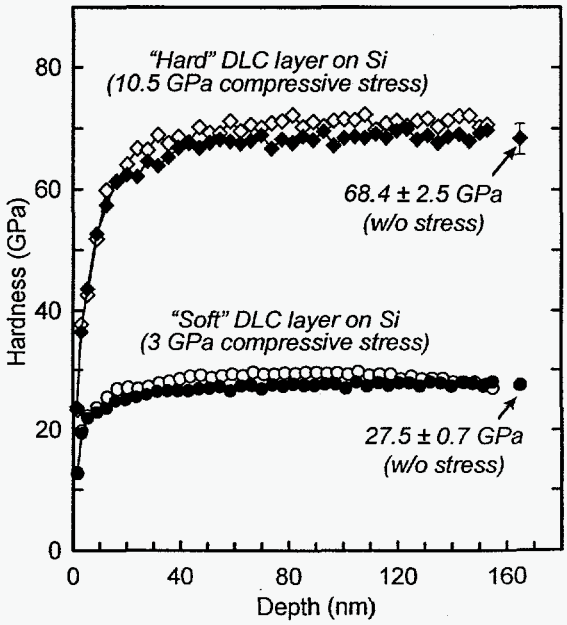

Figure 6. Calculated hardness for the two DLC samples: open symbols are the combined layer/substrate hardness, while filled symbols are for "bulk" simulations.

the "hard" layer indent shows that the stress reaches ~75 GPa just inside the indenter at the deepest penetration. The yield stress of crystalline diamond is difficult to determine, and probably depends on orientation and impurities [16], but one reference gives a value of 59 GPa [17]. The nanoindentation data for the "hard" DLC sample consists of 10 sequential indents, each done on a fresh spot on the surface. The data is exceptionally reproducible, with the curves overlaying almost exactly: the spread between indents of measured force at 150 nm is < 0.05 mN. Thus, if the indenter is deforming with each indent, the effect on the next indent is minimal. To test whether this experimental observation is consistent with a relatively low yield stress of the diamond indenter, we did a series of simulated indents of the "hard" layer with the indenter now modeled as an elastic-plastic material with a yield stress of 59 GPa. The force vs. depth curve for the first simulated indent was essentially identical to the result using no yielding. However, examination of the mesh afterward showed that the plastically deformed indenter had been additionally blunted by almost 8 nm. This simulated, deformed indenter shape was then used to replace the original indenter shape in the mesh, the indenter position was adjusted to again just touch the surface at the start (to match the experimental procedure), and the simulation was re-run. This time the force vs. depth curve was about 1 mN higher at 150 nm. Repeating the process gave successively higher forces, as the indenter was further blunted. Since this is very different from the experimental results, the diamond indenter cannot be yielding at 59 GPa.

The above procedure was repeated with a yield stress of 75 GPa for the diamond. The differences between successive simulations was much less (0.12 mN at 150 nm), but still significantly higher than the spread between experimental curves. Our conclusion is that the yield stress of diamond has a lower bound of 75 GPa. Although higher than expected from the literature, this result is consistent with the yield stresses and hardnesses measured here for the two DLC films. A linear extrapolation of the ratio of yield stress to hardness for these two samples to a hardness of 100 GPa for crystalline diamond gives an expected yield stress of 77 GPa for diamond.

Er-implanted Al(O)

The final example is an implanted sample which shows the flexibility of ABAQUS for modeling relatively complicated sample structures. The sample was formed by first depositing $Al_{90}O_{10}$ on Si using Al evaporation and an O plasma in an electron cyclotron resonance (ECR) plasma system, with the substrate at 100 °C and a bias of 300 V. The resulting layer was 854 nm thick, and nanoindentation testing with modeling showed a yield stress of 0.51 GPa and a relatively low Young's modulus of 49 GPa, with substantial scatter in the experimental curves. Transmission electron microscopy of similar layers shows some porosity, and this may be the reason for the scatter and low value of Young's modulus relative to that of pure Al, 72 GPa. The sample was then implanted with Er ions at multiple energies and doses: 8.0×10^{15}

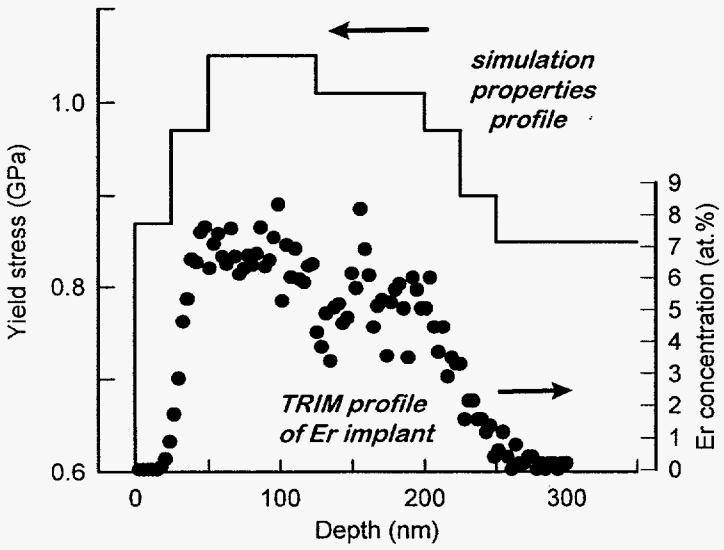

Figure 7. Er implant profile, calculated with TRIM, shown by solid circles, superimposed over the yield stress profile used in the simulation. Yield zero is offset.

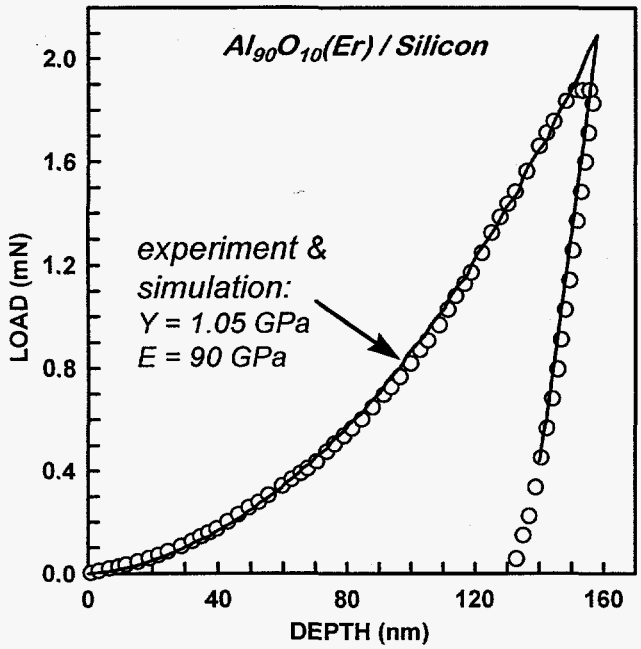

Figure 8. Experimental and calculated nanoindentation from Er-implanted Al(O) layer deposited on Si with ECR.

Er/cm^2 at 110 keV, 9.0x10^{15} at 190 keV, 1.9x10^{16} at 330 keV, and 3.5x10^{16} at 660 keV. The resulting profile, as calculated by TRIM [18], is shown in Fig. 7, with an average Er concentration of 6 at.%. Nanoindentation results from the implanted sample were modeled using multiple layers, each with its own property specification. The implanted region was modeled by 6 layers totaling 250 nm in depth, with yield stresses scaled to approximate the calculated implantation profile, including a thin region at the surface with very little Er. The following 604 nm, corresponding to unimplanted $Al_{90}O_{10}$, was modeled with constant properties, as was the Si substrate. The model yield stress as a function of depth is shown in Fig. 7 superimposed over the calculated Er profile. The values of yield stress vs. depth are those which gave the best fit: 0.85 GPa in the unimplanted region, rising to 1.05 GPa at the peak of the implanted region. Both values were required to obtain a fit along the entire loading portion of the curve. A Young's modulus of 90 GPa throughout the Al layer was also obtained by the fit. The simulation using these properties is shown in Figure 8, along with the experimental curve.

The implantation of Er substantially increased the yield stress, hardness and Young's modulus of the Al(O) layer. Contributing factors for the effect might be compressive stress induced by the implantation, increased inter-granular bonding due to atomic displacements during implantation, reduced porosity in the film, and hardening due to Er-O interactions. The effect and possible mechanisms are still under investigation.

SUMMARY

Nanoindentation is a very useful tool for determining mechanical properties at small scales, and is being used at many laboratories. However, application to deposited or ion-implanted thin films has been limited by the lack of convenient tools for modeling the non-linear sample response and extracting the layer properties. Our development of these tools has increased the applicability of nanoindentation testing to very thin layers, composite layers, and modulated compositions.

There are several uncertainties which might affect the results. Penetration of material cannot be modeled, so an indent of a very soft layer over a harder substrate may not be correctly simulated. The effect of creep is not modeled; the materials parameters we use are all time-independent. The strength of bonding between layer and substrate is also unknown; we assumed an unyielding interface. Finally, the precise shape of the indenter, particularly at very shallow indents, may not be sufficiently well known. However, even with all these modeling uncertainties considered, we judge the absolute uncertainty in our results to be no more than 20 %. This methodology is already impacting materials research programs at Sandia, such as surface treatments for Ni-based micro-electromechanical systems [9] and development of hard Al(O) alloys [2,19], and is expected to be transferred to several other laboratories around the country.

ACKNOWLEDGMENTS

Technical assistance by K. G. Minor and M. P. Moran is gratefully acknowledged. Careful nanoindentation measurements by Barry Lucas at Nano Instruments are appreciated. This work was performed at Sandia National Laboratories under the auspices of the U.S. Department of Energy and funded by its Office of Basic Energy Sciences, Div. of Materials Sciences, under contract no. DE-AC04-94AL85000. Much of the work was supported as part of the BES Synthesis and Processing Center's project on Processing for Surface Hardness. Visual Basic and Excel are trademarks of Microsoft, Inc.

REFERENCES

1. ABAQUS version 5.5, Hibbitt, Karlsson & Sorensen, Inc., Pawtucket, RI.
2. J. A. Knapp, D. M. Follstaedt, and S. M. Myers, J. Appl. Phys. **79** (1996) 1116.
3. J. A. Knapp and D. M. Follstaedt, Mat. Res. Soc. Symp. Proc. **397** (1996) in press.
4. J. A. Knapp, D. M. Follstaedt, J. C. Barbour and S. M. Myers, Proc. of the 1996 Int. Ion Beam Modification of Materials conference, in press.
5. All of the nanoindentation tests were performed at Nano Instruments, Inc., Knoxville, TN.
6. W. C. Oliver and G. M. Pharr, J. Mater. Res. **7** (1992) 1564.
7. D. M. Follstaedt, Nucl. Instrum. Methods **B10-11**, (1985) 549.
8. Mechanical Behavior of Materials, eds. F. A. McClintock and A. S. Argon (Addison-Wesley, Reading, MA, 1966) pp. 276-279.
9. S. M. Myers, D. M. Follstaedt, J. A. Knapp and T. R. Christenson, Mat. Res. Soc. Symp. Proc. **444** (1997) in press.
10. J. Niebuhr, R. Gerber, A. Schaller and H.-W. Müller, Physical Data of Amorphous Metals, Par B (Fachinformationszentrum Karlsruhe, Germany, 1991).
11. A. Inoue, T. Iwadachi, T. Minemura and T. Masumoto, Trans. Jap. Inst. Metals **22** (1981) 197.
12. D. R. McKenzie, D. Muller and B. A. Pailthorpe, Phys. Rev. Lett. **67**, (1991) 773.
13. S. Anders, A. Anders, J. W. Ager III, Z. Wang, G. M. Pharr, T. Y. Tsui, I. G. Brown and C. S. Bhatia, Mat. Res. Soc. Symp. **383** (1995) 453.
14. S. Anders, A. Anders, I. G. Brown, B. Wei, K. Komvopoulos, J. W. Ager III, K. M. Yu, Surf. Coatings Technol. **68/69** (1994) 388.
15. G. M. Pharr, T. Y. Tsui, A. Bolshakov and W. C. Oliver, Mat. Res. Soc. Symp. Proc. **338** (1994) 127.
16. C. A. Brookes in The Properties of Natural and Synthetic Diamond, edited by J. E. Field (Academic, New York, 1992) pp. 515-546.
17. J. Robertson, Phys. Rev. Lett. **68** (1992) 220.
18. TRIM computer code, J. F. Ziegler, IBM Research Center, Yorktown Heights, New York; See also, J. F. Ziegler, J. P. Biersack and U. Littmark, The Stopping and Range of Ions in Solids, vol. 1 (Pergamon, New York, 1985).
19. D. M. Follstaedt, J. A. Knapp, J. C. Barbour, S. M. Myers and M. T. Dugger, Mat. Res. Soc. Symp. Proc. **457** (1997) in press.